Applied Mathematics and Mechanics
(English Edition, Vol. 17, No. 7, July 1996)

Published by SU,
Shanghai, China

THE ANALYTICAL STUDY ON THE LASER INDUCED REVERSE-PLUGGING EFFECT BY USING THE CLASSICAL ELASTIC PLATE THEORY (II)——REVERSE-BULGE MOTION

Zhou Yichun (周益春)[1] Duan Zhuping (段祝平)[1] Xie Bomin (解伯民)[1]

Abstract

The reverse-bulge motion (RBM) in the metallic foils, which is induced by spatially cylindrical long pulse laser, is examined in order to analyse the newly-discovered reverse-plugging effect (RPE). An uncoupled, thin plate theory is used to determine the induced flexural vibrations. The solution is obtained as the superposition of two displacement fields, representing the quasi-static and the dynamic behaviors. Meanwhile, the equivalent thermal loading and the dimensionless analysis of thin plate motion are presented. Numerical results presented may partially explain the RBM of thin plate at the early stage of laser irradiation.

Key words long-pulsed laser beam, the RPE, the RBM, thermal-elastic thin-plate theory

I. Introduction

A new type of damage, i. e. the RPE in studying the interaction of a single-mode long-pulsed Nd: Glass laser beam with copper and aluminum foils has been reported[1-2]. The RPE is different from the well-known damage types which are melting, vaporization and shock waves in materials. The process of the RPE in metallic foils induced by long-pulsed laser is divided into three macroscopic stages, i. e. the reverse-bulge formation, shear deformation localization and perforation. The RPE is also a typical 3 - F (Flow-Fracture-Fragmentation) process. The temperature distribution analysis has shown that the temperature gradient in the axial direction is the key factor to induce the RBM. The discontinuity of temperature and its gradient on the rim of laser spot in the radial direction is the key factor to induce shear deformation localization[3].

Based on the temperature field analysis in[3], the present study explores the characteristics of the RBM in the metallic foils irradiated by a spatially cylindrical type long-pulse laser beam, where the classical thin-plate theory is used. The exact solution is derived as the superposition of two displacement fields, representing the quasi-static and the dynamic behaviors. In Section II, the theoretical considerations and the governing equations are outlined. In Section III, the quasi-static behavior of the transverse motion is obtained. In Section IV, the dynamic behavior of the transverse motion is investigated by using the Hankel transform and Laplace transform. Some numerical results, discussions and dimensionless

[1] Laboratory for Nonlinear Mechanics of Continuous Media (LNM), Institute of Mechanics, Chinese Academy of Sciences, Beijing 100080, P. R. China

analysis are detailed in Section V. We conclude in Section VI with a summary of the main feartures of the present study.

II. Governing Equations

In the present study the transverse deflection of a thin plate irradiated by a pulse laser beam can be modelled on the basis of the assumptions:

(1) The thermal-mechanical coupling effect is neglected. The neglect of thermoelastic coupling is generally justifiable for the problems in which thermoelastic dissipation is not of primary interest[4].

(2) We shall confine ourselves to the infinitesimal deformation theory. And thus, the effect of membrane force and shear force on the transverse deflection and their coupling effect are ignored.

(3) All the material parameters are constant. This implies that the temperature-dependence of parameters is neglected.

However, although the assumptions (2) and (3) may be invalid for the whole process of the PRE, they should be reasonable for the RBM. According to the classical (Kirchhoff) plate theory, the transverse displacement of the plate middle plane, as described in Fig. 3 in [3], is governed by the equations as follows:

$$D_1\Delta^2 w+\frac{1}{1-\nu}\Delta M_t+\rho h\frac{\partial^2 w}{\partial t^2}=0 \tag{2.1}$$

initial condition

$$w\Big|_{t=0}=\frac{\partial w}{\partial t}\Big|_{t=0}=0 \tag{2.2}$$

boundary condition

$$w\Big|_{r=b}=\frac{\partial w}{\partial r}\Big|_{r=b}=0 \tag{2.3}$$

where $\triangle$ is the Laplace operator, w represents the transverse displacement of the plate middle plane, $D_1=Eh^3/12(1-\nu^2)$ denotes the bending stiffness, and E, ν, ρ denote, respectively, the Young's modulus, Poisson ratio and mass density. Other notations are defined in [3]. The thermal moment or equivalent external loading in Eq. (2.1) is defined in term of the temperature rise $\theta(r, z, t)$ by

$$M_t=\alpha_0 E\int_{-h/2}^{h/2}\theta(r,z,t)z\,dz \tag{2.4}$$

where α_0 is the coefficient of thermal expansion.

For the convenience in the subsequent analysis, we introduce the following dimensionless variables

$$\hat{\theta}=\frac{\theta}{h_4 T_m},\quad \hat{w}=\frac{w}{w_0 a},\quad \hat{M}_t=\frac{M_t}{\frac{1}{4}h^2\rho_0 M_p},$$

$$\hat{M}_r=\frac{M_r}{\frac{1}{4}h^2\sigma_0 m_0},\quad \hat{M}_\theta=\frac{M_\theta}{\frac{1}{4}h^2\sigma_0 m_0} \tag{2.5}$$

Also, the basic dimensionless parameters are defined as

$$h_1=\frac{h}{a},\quad A=\frac{\alpha a^2}{D},\quad B=\frac{(\alpha+\beta)a^2}{D},\quad h_3=\alpha_0 T_m$$

$$h_4=\frac{I_{max}a}{k_0 T_m}=\frac{(1-R_0)P_{max}}{k_0\pi a T_m},\quad h_5=\frac{E}{\sigma_0},\quad h_6=\frac{\rho D^2}{aE} \tag{2.6}$$

Meanwhile, the following dimensionless parameters are used in the present study

$$w_p=24(1+\nu)h_3h_4,\quad M_p=8h_3h_4h_5,\quad m_0=8h_1h_3h_4h_6/(1-\nu)$$
$$m_1=12(1-\nu^2)h_6/h_1^2 \tag{2.7}$$

where σ_0 is the yield strength at ambient temperature, M_r and M_θ are, respectively, the bending moments in the radial and circumferential directions,

$$M_r=-D_1\left(\frac{\partial^2 w}{\partial r^2}+\frac{\nu}{r}\frac{\partial w}{\partial r}\right)-\frac{M_t}{1-\nu} \tag{2.8}$$

$$M_\theta=-D_1\left(\frac{1}{r}\frac{\partial w}{\partial r}+\nu\frac{\partial^2 w}{\partial r^2}\right)-\frac{M_t}{1-\nu} \tag{2.9}$$

For the convenience of writing in the subsequent derivation, the dimensionless variables $\hat{\theta}$, $\hat{w}$, $\hat{M}_t$, $\hat{M}_r$, $\hat{M}_\theta$, $\hat{r}$ and $\hat{z}$ are, respectively, replaced by θ, w, M_t, M_r, M_θ, r and z. Therefore, the governing equations of the RBM are expressed in dimensionless form as follows:

$$\Delta^2 w+\frac{1}{h_1}\Delta M_t+m_1\frac{\partial^2 w}{\partial t^2}=0 \tag{2.10}$$

initial conditions

$$w\Big|_{t=0}=\frac{\partial w}{\partial t}\Big|_{t=0}=0 \tag{2.11}$$

boundary conditions

$$w\Big|_{r=h_2}=\frac{\partial w}{\partial r}\Big|_{r=h_2}=0 \tag{2.12}$$

The dimensionless thermal moment M_t is rewritten as

$$M_t=\frac{1}{2h_1^2}\int_{-h_1^2/2}^{h_1^2/2}\theta z\,dz \tag{2.13}$$

Just as in the previous investigations[5-6], the deflection w is regarded as the sum of two terms, namely,

$$w=w_s+w_d \tag{2.14}$$

where w_s and w_d represent, respectively, the quasi-static deflection and dynamic deflection. The quasi-static deflection w_s satisfies the differential equation

$$\Delta^2 w_s+\frac{1}{h_1}\Delta M_t=0 \tag{2.15}$$

together with the prescribed boundary conditions

$$w_s\Big|_{r=h_2}=\frac{\partial w_s}{\partial r}\Big|_{r=h_2}=0 \tag{2.16}$$

The dynamic deflection w_d must then satisfy the equation

$$\Delta^2 w_d+m_1\frac{\partial^2 w_s}{\partial t^2}+m_1\frac{\partial^2 w_d}{\partial t^2}=0 \tag{2.17}$$

together with the boundary conditions

$$w_d\Big|_{r=h_2}=\frac{\partial w_d}{\partial r}\Big|_{r=h}=0 \tag{2.18}$$

In addition, the initial conditions should be expressed as follows

$$w_d\Big|_{t=0}=-w_s\Big|_{t=0},\qquad \frac{\partial w_d}{\partial t}\Big|_{t=0}=-\frac{\partial w_s}{\partial t}\Big|_{t=0} \tag{2.19}$$

Consequently, (2.14)−(2.19) are the basic governing equations of dimensionless deflection w. Substituting some dimensionless variables into (2.8) and (2.9), the dimensionless bending moments M_r and M_θ are expressed as follows

$$M_r=-\left(\frac{\partial^2 w}{\partial \rho^2}+\frac{\nu}{r}\frac{\partial w}{\partial r}+\frac{M_t}{h_1}\right) \tag{2.20}$$

$$M_\theta=-\left(\nu\frac{\partial^2 w}{\partial r^2}+\frac{1}{r}\frac{\partial w}{\partial r}+\frac{M_t}{h_1}\right) \tag{2.21}$$

III. Quasi-Static Solution

Substituting the dimensionless temperature rise expression (44) in [3] into the dimensionless thermal moment expression (2.13), we have

$$M_t=-\frac{h_1}{h_2^2}\sum_{k_n}\frac{J_0(k_n r)f^*(k_n)}{J_1^2(k_n h_2)}\bar{g}(k_n,t) \tag{3.1}$$

where the $\bar{g}(k_n,\ t)$ is expressed as

$$\bar{g}(k_n,t)=\frac{1}{24}g(t)+2\sum_{m=1}^{\infty}\frac{[(-1)^m-1]}{(m\pi)^4}\Big[g(t)$$

$$-\left(\frac{m\pi}{h_1}\right)^2\left(\frac{\exp[-At]-\exp[-Ct]}{C-A}-\frac{\exp[-Bt]-\exp[-Ct]}{C-B}\right)\Big] \tag{3.2}$$

For Eq. (2.15), we have

$$\frac{h_1}{r}\frac{\partial}{\partial r}\left\{r\frac{\partial}{\partial r}\left[\frac{1}{r}\frac{\partial}{\partial r}\left(r\frac{\partial w_s}{\partial r}\right)\right]\right\}+\frac{1}{r}\frac{\partial}{\partial r}\left(r\frac{\partial M_t}{\partial r}\right)=0 \tag{3.3}$$

Integrating Eq. (3.3) and referring to the finiteness of w_s and $\frac{\partial w_s}{\partial r}$ at the point $r=0$, we obtain

$$w_s=\frac{1}{4}C_1 r^2-\frac{1}{h_2^2}\sum_{k_n}\frac{J_0(k_n r)f^*(k_n)}{k_n^2 J_1^2(k_n h_2)}\bar{g}(k_n,t)+C_2 \tag{3.4}$$

where C_1 and C_2 are integral constants which are determined with boundary conditions (2.16). Then we have

$$w_s=-\frac{1}{h_2^2}\sum_{k_n}\frac{f^*(k_n)g(k_n,t)}{k_n^2J_1^2(k_nh_2)}\left[J_0(k_nr)+\frac{1}{2h_2}k_nJ_1(k_nh_2)(r^2-h_2^2)\right] \tag{3.5}$$

In order to understand the characteristics of the quasi-static bending moments distribution, we insert (3.5) into (2.20)−(2.21) and obtain the dimensionless bending moments

$$M_r=\frac{1}{h_2^2}\sum_{k_n}\frac{f^*(k_n)g(k_n,t)}{k_nJ_1^2(k_nh_2)}\left[\frac{1+\nu}{h_2}J_1(k_nh_2)+\frac{1-\nu}{r}J_1(k_nr)\right] \tag{3.6}$$

$$M_\theta=\frac{1}{h_2^2}\sum_{k_n}\frac{f^*(k_n)g(k_n,t)}{k_nJ_1^2(k_nh_2)}\left[(1-\nu)k_nJ_0(k_nr)\right.$$
$$\left.+\frac{1+\nu}{h_2}J_1(k_nh_2)-\frac{1-\nu}{r}J_1(k_nr)\right] \tag{3.7}$$

IV. Dynamic Solution

To obtain an exact solution to Eq. (2.17) together with the prescribed boundary conditions (2.18) and the initial conditions (2.19), the dynamic deflection w_d is expanded in following form

$$w_d=\sum_{a_n}w_d^*(a_n,t)\left[I_0(a_nr)-\frac{I_0(a_nh_2)}{J_0(a_nh_2)}J_0(a_nr)\right] \tag{4.1}$$

where a_n are the roots of the following equation

$$J_0(a_nh_2)I_1(a_nh_2)+J_1(a_nh_2)I_0(a_nh_2)=0 \tag{4.2}$$

and I_n, J_n are, respectively, the n-th order imaginary variable Bessel function and the n-th order Bessel function. Setting y_n as

$$y_n=I_0(a_nr)-\frac{I_0(a_nh_2)}{J_0(a_nh_2)}J_0(a_nr) \tag{4.3}$$

utilizing repeatedly the Bessel equation and some transforms, we prove readily that the eigenfunctions y_n are complete and orthogonal, that is;

$$\int_0^{h_2}y_my_nrdr=0 \qquad (m\neq n) \tag{4.4}$$

In order to solve exactly the dynamic deflection w_d, the modulus and some transforms are derived in the following.

1. The derivation of modulus $\int_0^{h_2}y_n^2rdr$

Substituting (4.3) into the expression of modulus $\int_0^{h_2}y_n^2rdr$ we obtain

$$\int_0^{h_2}y_n^2rdr=\int_0^{h_2}\left[I_0^2(a_nr)+\frac{I_0^2(a_nh_2)}{J_0^2(a_nh_2)}J_0^2(a_nr)-\frac{2I_0(a_nh_2)}{J_0(a_nh_2)}I_0(a_nr)J_0(a_nr)\right]rdr \tag{4.5}$$

According to the following expression

$$\int_0^{h_2} I_0^2(\alpha_n r)\,rdr=\frac{1}{2}h_2^2 I_0^2(\alpha_n h_2)-\int_0^{h_2} r^2 I_0(\alpha_n r)\frac{dI_0(\alpha_n r)}{dr}dr \tag{4.6}$$

and the imaginary variable Bessel equation,

$$r^2\frac{d^2I_0(\alpha_n r)}{dr^2}+r\frac{dI_0(\alpha_n r)}{dr}-\alpha_n^2 r^2 I_0(\alpha_n r)=0 \tag{4.7}$$

utilizing Eq. (4.7) and some transforms, we obtain

$$\int_0^{h_2} I_0^2(\alpha_n r)rdr=\frac{1}{2}h_2^2[I_0^2(\alpha_n h_2)-I_1^2(\alpha_n h_2)] \tag{4.8}$$

Similarly, utilizing the Bessel Equation

$$r^2\frac{d^2J_0(\alpha_n r)}{dr^2}+r\frac{dJ_0(\alpha_n r)}{dr}+\alpha_n^2 r^2 J_0(\alpha_n r)=0 \tag{4.9}$$

we obtain easily

$$\int_0^{h_2} J_0^2(\alpha_n r)rdr=\frac{1}{2}h_2^2[J_0^2(\alpha_n h_2)+J_1^2(\alpha_n h_2)] \tag{4.10}$$

$$\int_0^{h_2} I_0(\alpha_n r)J_0(\alpha_n r)rdr=0 \tag{4.11}$$

Substituting (4.8), (4.10) and (4.11) into (4.5), and referring to Eq. (4.2), we obtain the modulus as follows

$$\int_0^{h_2} y_n^2 rdr=h_1^2 I_0^2(\alpha_n h_2) \tag{4.12}$$

2. The transform coefficients

(1) $\int_0^{h_2} J_0(k_n r)y_n(\alpha_n r)rdr$

Substituting (4.3) into the above expression, we have

$$\int_0^{h_2} J_0(k_n r)y_n(\alpha_n r)rdr=\int_0^{h_2} J_0(k_n r)\left[I_0(\alpha_n r)-\frac{I_0(\alpha_n h_2)}{J_0(\alpha_n h_2)}J_0(\alpha_n r)\right]rdr \tag{4.13}$$

Utilizing the Bessel Eq. (4.7) and the following equation,

$$r^2\frac{d^2J_0(k_n r)}{dr^2}+r\frac{dJ_0(k_n r)}{dr}+k_n^2 r^2 J_0(k_n r)=0 \tag{4.14}$$

we have

$$-(k_n^2+\alpha_n^2)rI_0(\alpha_n r)J_0(k_n r)=\frac{d}{dr}\left[rI_0(\alpha_n r)\frac{dJ_0(k_n r)}{dr}-r\frac{dI_0(\alpha_n r)}{dr}J_0(k_n r)\right] \tag{4.15}$$

Consequently, we obtain

$$\int_0^{h_2} rI_0(\alpha_n r)J_0(k_n r)dr=\frac{h_2 k_n}{k_n^2+\alpha_n^2}I_0(\alpha_n h_2)J_1(k_n h_2) \tag{4.16}$$

where the identity $J_0(k_n h_2)=0$ is used. Similarly, we obtain the following expression

$$\int_0^{h_2} rJ_0(\alpha_n r)J_0(k_n r)dr=\frac{h_2 k_n}{k_n^2-\alpha_n^2}J_0(\alpha_n h_2)J_1(k_n h_2) \tag{4.17}$$

Finally, we have the following transform coefficient,

$$\int_0^{h_2} J_0(k_n r)y_n(\alpha_n r)rdr=-\frac{2h_2 k_n \alpha_n^2}{k_n^4-\alpha_n^4}I_0(\alpha_n h_2)J_1(k_n h_2) \tag{4.18}$$

(2) $\int_0^{h_2}(h_2^2-r^2)y_n(\alpha_n r)rdr$

According to the following expressions

$$\int_0^{h_2} I_0(\alpha_n r)rdr=\frac{h_2}{\alpha_n}I_1(\alpha_n h_2),\qquad \int_0^{h_2} J_0(\alpha_n r)rdr=\frac{h_2}{\alpha_n}J_1(\alpha_n h_2) \tag{4.19}$$

we have

$$\int_0^{h_2} y_n(\alpha_n r)rdr=\frac{2h_2}{\alpha_n}I_1(\alpha_n h_2) \tag{4.20}$$

$$\int_0^{h_2} I_0(\alpha_n r)r^3dr=\frac{h_2^3}{\alpha_n}I_1(\alpha_n h_2)-\frac{2h_2^2}{\alpha_n^2}I_0(\alpha_n h_2)+\frac{4h_2}{\alpha_n^3}I_1(\alpha_n h_2) \tag{4.21}$$

$$\int_0^{h_2} J_0(\alpha_n r)r^3dr=\frac{h_2^3}{\alpha_n}J_1(\alpha_n h_2)+\frac{2h_2^2}{\alpha_n^2}J_0(\alpha_n h_2)-\frac{4h_2}{\alpha_n^3}J_1(\alpha_n h_2) \tag{4.22}$$

Finally, we have the following transform coefficient,

$$\int_0^{h_2}(h_2^2-r^2)y_n(\alpha_n r)rdr=\frac{4h_2^2}{\alpha_n^2}I_0(\alpha_n h_2) \tag{4.23}$$

3. Transform coefficient $w_d^*(\alpha_n,t)$

Substituting expression (4.1) into Eq. (2.17), we have the following equation on the unknown variable $w_d^*(\alpha_n,t)$

$$\sum_{\alpha_n}\alpha_n^4 w_d^*(\alpha_n,t)y_n(\alpha_n r)+m_1\sum_{\alpha_n}\frac{d^2w_d^*(\alpha_n,t)}{dt^2}y_n(\alpha_n r)+m_1\frac{\partial^2 w_s}{\partial t^2}=0 \tag{4.24}$$

Referring to the orthogonality of the eigenfunction y_n, the right side and the left side of Eq. (4.24) times, simultaneously, $y_n(\alpha_n r)r$ and integrating them, meanwhile substituting the modulus (4.12) into the new equation, finally, we obtain the ordinary differential equation on the unknown variable $w_d^*(\alpha_n, t)$ as follows

$$\alpha_n^4 h_2^2 I_0^2(\alpha_n h_2)w_d^*(\alpha_n,t)+m_1 h_2^2 I_0^2(\alpha_n h_2)\frac{d^2w_d^*(\alpha_n,t)}{dt^2}+m_1\int_0^{h_2}\frac{\partial^2 w_s}{\partial t^2}y_n rdr=0 \tag{4.25}$$

Substituting (4.18) and (4.23) into the last term on the left side of Eq. (4.25), we have

$$\int_0^{h_2}\frac{d^2w_s}{dt^2}y_n rdr=\frac{2}{h_2}\sum_{k_n}\frac{f^*(k_n)}{J_1(k_n h_2)}\frac{k_n^3 I_0(\alpha_n h_2)}{(k_n^4-\alpha_n^4)\alpha_n^2}\frac{d^2\bar{g}(k_n,t)}{dt^2} \tag{4.26}$$

Furthermore, we obtain the ordinary differential equation as follows

$$\frac{d^2w_d^*}{dt^2}+\frac{\alpha_n^4}{m_1}w_d^*+\sum_{k_n}\frac{\alpha_n^2}{\sqrt{m_1}}F(k_n,\alpha_n)\frac{d^2\bar{g}(k_n,t)}{dt^2}=0 \tag{4.27}$$

where

$$F(k_n,\alpha_n)=\frac{2}{h_2^3}\frac{\sqrt{m_1}k_n^3f^*(k_n)}{J_1(k_nh_2)I_0(\alpha_nh_2)(k_n^4-\alpha_n^4)\alpha_n^2} \tag{4.28}$$

Using Eq. (3.2) and the following formula

$$\frac{1}{24}+2\sum_{m=1}^{\infty}\frac{[(-1)^m-1]}{(m\pi)^4}=0 \tag{4.29}$$

we have

$$\bar{g}\Big|_{t=0}=0 \qquad \frac{d\bar{g}}{dt}\Big|_{t=0}=0 \tag{4.30}$$

Consequently, referring to Eq. (4.27) we have the transform coefficient $w_d^*(\alpha_n,t)$ as follows

$$w_d^*(\alpha_n,t)=C_n(t)\cos\left(\frac{\alpha_n^2}{\sqrt{m_1}}t\right)+D_n(t)\sin\left(\frac{\alpha_n^2}{\sqrt{m_1}}t\right) \tag{4.31}$$

where

$$C_n(t)=\int_0^t\sum_{k_n}F(k_n,\alpha_n)\frac{d^2\bar{g}(k_n,t')}{dt^2}\sin\left(\frac{\alpha_n^2}{\sqrt{m_1}}t'\right)dt' \tag{4.32}$$

$$D_n(t)=-\int_0^t\sum_{k_n}F(k_n,\alpha_n)\frac{d^2g(k_n,t')}{dt'^2}\cos\left(\frac{\alpha_n^2}{\sqrt{m_1}}t'\right)dt' \tag{4.33}$$

Setting the notations $L_1(\eta)$ and $L_2(\eta)$ as

$$L_1(\eta)=\int_0^t\exp[-\eta t']\sin\left(\frac{\alpha_n^2}{\sqrt{m_1}}t'\right)dt' \tag{4.34}$$

$$L_2(\eta)=\int_0^t\exp[-\eta t']\cos\left(\frac{\alpha_n^2}{\sqrt{m_1}}t'\right)dt' \tag{4.35}$$

we obtain

$$L_1(\eta)=\frac{1}{1+\frac{1}{\eta^2}\frac{\alpha_n^4}{m_1}}\left[\frac{1}{\eta^2}\frac{\alpha_n^2}{\sqrt{m_1}}-\frac{1}{\eta}\exp[-\eta t]\sin\left(\frac{\alpha_n^2}{\sqrt{m_1}}t\right)\right.$$
$$\left.-\frac{1}{\eta^2}\frac{\alpha_n^2}{\sqrt{m_1}}\exp[-\eta t]\cos\left(\frac{\alpha_n^2}{\sqrt{m_1}}t\right)\right] \tag{4.36}$$

$$L_2(\eta)=\frac{1}{1+\frac{1}{\eta^2}\frac{\alpha_n^4}{m_1}}\left[\frac{1}{\eta}-\frac{1}{\eta}\exp[-\eta t]\cos\left(\frac{\alpha_n^2}{\sqrt{m_1}}t\right)\right.$$
$$\left.+\frac{1}{\eta^2}\frac{\alpha_n^2}{\sqrt{m_1}}\exp[-\eta t]\sin\left(\frac{\alpha_n^2}{\sqrt{m_1}}t\right)\right] \tag{4.37}$$

Substituting (3.2) into (4.32) and (4.33), we obtain, respectively, the following expressions

$$E_1(\alpha_n,k_n,t)=\int_0^t \frac{d^2\bar{g}(k_n,t')}{dt'^2}\sin\left(\frac{\alpha_n^2}{\sqrt{m_1}}t'\right)dt'$$

$$=\frac{1}{24}[A^2L_1(A)-B^2L_1(B)]+2\sum_{m=1}^{\infty}\frac{[(-1)^m-1]}{(m\pi)^4}\{A^2L_1(A)-B^2L_1(B)$$

$$-\left(\frac{m\pi}{h_1}\right)^2\left[\frac{A^2L_1(A)-C^2L_1(C)}{C-A}-\frac{B^2L_1(B)-C^2L_1(C)}{C-B}\right]\} \tag{4.38}$$

$$E_2(\alpha_n,k_n,t)=\int_0^t \frac{d^2\bar{g}(k_n,t')}{dt'^2}\cos\left(\frac{\alpha_n^2}{\sqrt{m_1}}t'\right)dt'$$

$$=\frac{1}{24}[A^2L_2(A)-B^2L_2(B)]+2\sum_{m=1}^{\infty}\frac{[(-1)^m-1]}{(m\pi)^4}\left\{A^2L_2(A)-B^2L_2(B)\right.$$

$$\left.-\left(\frac{m\pi}{h_1}\right)^2\left[\frac{A^2L_2(A)-C^2L_2(C)}{C-A}-\frac{B^2L_2(B)-C^2L_2(C)}{C-B}\right]\right\} \tag{4.39}$$

Finally, we have

$$w_d^*(\alpha_n,t)=\left[\sum_{k_n}F(k_n,\alpha_n)E_1(\alpha_n,k_n,t)\right]\cos\left(\frac{\alpha_n^2}{\sqrt{m_1}}t\right)$$

$$-\left[\sum_{k_n}F(k_n,\alpha_n)E_2(\alpha_n,k_n,t)\right]\sin\left(\frac{\alpha_n^2}{\sqrt{m_1}}t\right) \tag{4.40}$$

Consequently, inserting (4.40) into (4.1), we obtain the exact solution of dynamical deflection w_d in the following

$$w_d=\sum_{\alpha_n}\left\{F(k_n,\alpha_n)E_1(\alpha_n,k_n,t)\right]\cos\left(\frac{\alpha_n^2}{\sqrt{m_1}}t\right)-\left[\sum_{k_n}F(k_n,\alpha_n)E_2(\alpha_n,k_n,t)\right]$$

$$\sin\left(\frac{\alpha_n^2}{\sqrt{m_1}}t\right)\Big\}\left[I_0(\alpha_n r)-\frac{I_0(\alpha_n h_2)}{J_0(\alpha_n h_2)}J_0(\alpha_n r)\right] \tag{4.41}$$

Finally, substituting (4.1) and (4.41) into (2.14) we obtain the exact solution of dimensionless deflection w.

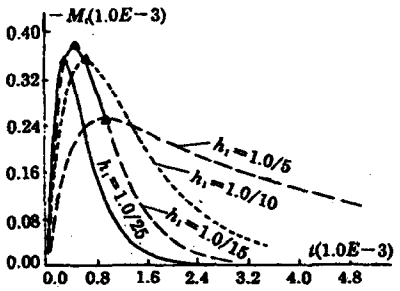

Fig. 1 Histories of M_r at point $r=0$ with different values of h_1

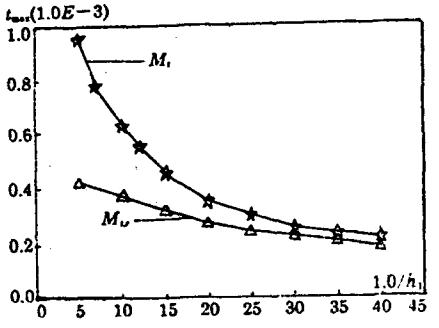

Fig. 2 The variation of T_{max1} and T_{max2} with h_1^{-1}, where T_{max1} and T_{max2} are, respectively, the time, when M_r at point ($r=0$) and $\partial M_r/\partial r$ on the rim of laser spot reach their maximum values

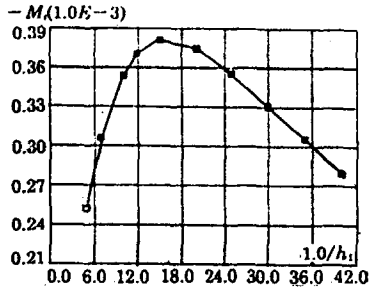

Fig. 3 The variation of $M_{r\max}$ with h_1^{-1}, where $M_{r\max}$ is the maximum value of M_r at the point $r=0$

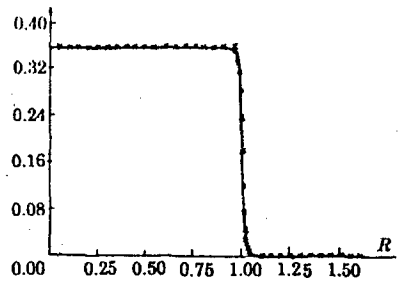

Fig. 4 The variation of M_r with r, where $t=3.7\times10^{-4}$ and $h_1^{-1}=25$

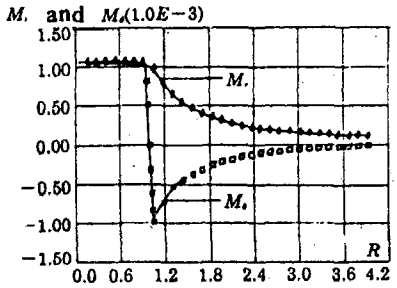

Fig. 5 The variation of M_r and M_θ with r, where $t=1.5\times10^{-4}$ and $h_1^{-1}=25$

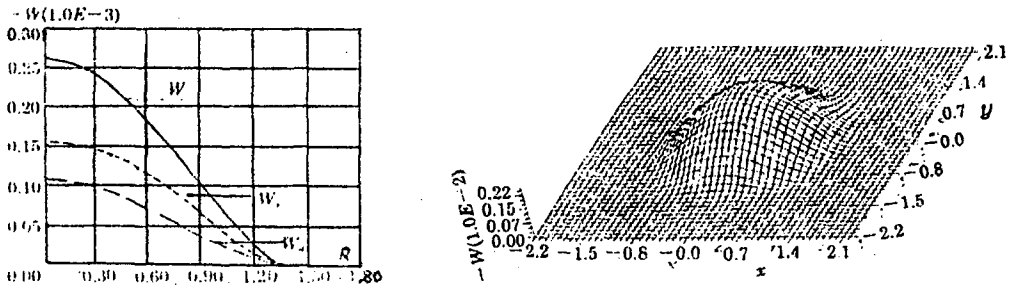

(a) two-dimensional shape (b) three-dimensional shape

Fig. 6 Deflected shape of the middle plane of a thin plate, where $t=3.0\times10^{-4}$ and $h_1^{-1}=25$

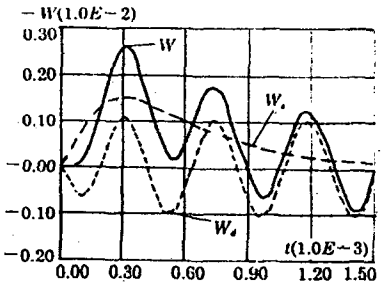

Fig. 7 The histories of w_r, w_θ and w at the point $r=0$, where $h_1^{-1}=25$

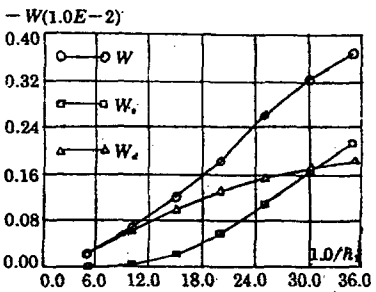

Fig. 8 The variations of $w_{r\max}$, $w_{\theta\max}$ and $w_{\max}$ with h_1^{-1}, where $w_{r\max}$, $w_{\theta\max}$ and $w_{\max}$ are, respectively, the maximum values of w_r, w_θ and w at the point $r=0$

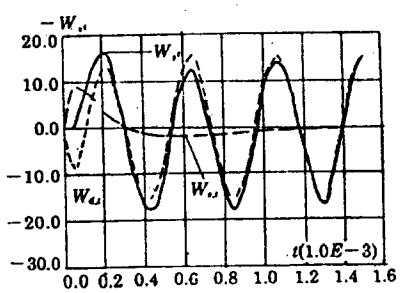

Fig. 9 The histories of $\frac{\partial w}{\partial t}$, $\frac{\partial w_s}{\partial t}$ and $\frac{\partial w_d}{\partial t}$ at the point $r=0$

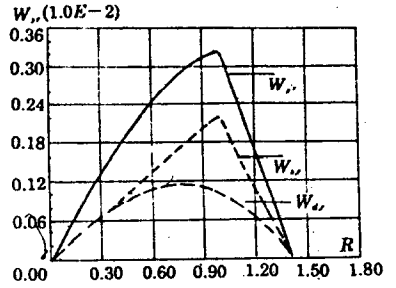

Fig. 10 The variations of $\frac{\partial w}{\partial r}$, $\frac{\partial w_s}{\partial r}$ and $\frac{\partial w_d}{\partial r}$ with r

V. Calculated Results and Discussions

Experimental results[1-2] and the analysis of temperature fields show that only the spatially cylindrical distribution of laser offers a formidable potential for the RPE. Consequently, the spatially cylindrical laser beam, which was described in Fig. 2 in [3], is supposed in the present study. Meanwhile, the temporal shape is expressed as formula (22) in [3] and the target material is H65 copper alloy foils. The characteristics of the thermal moments, the transverse deflection and the quasi-static bending moments are analyzed in the following.

1. Dimensionless analysis

The characteristics of the RBM, i. e., the motion state at the early stage of laser irradiation, are determined by the laser parameters, the material parameters and the geometric parameters. In other words, there is the following implicit function

$$\Psi[h,a,\alpha,D,(\alpha+\beta),\alpha_0,T_m,I_{max}/k_0,E,\sigma_0,\rho]=0 \tag{5.1}$$

where $I_{max}=(1-R_0)P_{max}/\pi a^2$ is the maximum laser intensity absorbed by the target. If the dimensions of distance $[L]$, time $[T]$, mass $[M]$ and temperature $[K]$ are selected as basic dimensions, the dimensions of these variables are:

$$\begin{aligned}&[h]=[L]\quad[a]=[L]\quad[\alpha]=[T^{-1}]\quad[D]=[L^2T^{-1}]\quad[(\alpha+\beta)]=[T^{-1}]\\&[\alpha_0]=[K^{-1}]\quad[T_m]=[K]\quad[I_{max}/k_0]=[KL^{-1}]\quad[E]=[ML^{-1}T^{-2}]\\&[\sigma_0]=[ML^{-1}T^{-2}]\quad[\rho]=[ML^{-3}]\end{aligned} \tag{5.2}$$

According to the Π theorem, we have

$$\Phi[h^{x_1}a^{x_2}\alpha^{x_3}D^{x_4}(\alpha+\beta)^{x_5}\alpha_0^{x_6}T_m^{x_7}(I_{max}/k_0)^{x_8}E^{x_9}\sigma_0^{x_{10}}\rho^{x_{11}}]=0 \tag{5.3}$$

Substituting the dimension of each variable in (5.2) into Eq. (5.3), and let the factors of $[L]$, $[T]$, $[M]$ and $[K]$ on the left part of Eq. (5.3), respectively, be zero, we obtain the following four equations:

$$x_1+x_2+2x_4-x_8-x_9-x_{10}-3x_{11}=0 \tag{5.4}$$

$$x_3+x_4+x_6+2x_9+2x_{10}=0 \tag{5.5}$$

$$x_9+x_{10}+x_{11}=0 \tag{5.6}$$

$$-x_8+x_7+x_8=0 \tag{5.7}$$

From Eqs. (5.4)−(5.7), eliminating x_2, x_4, x_7 and x_9, we have the following expression

$$\Psi\{(h/a)^{\pi_1}(a\alpha^2/D)^{\pi_2}[(\alpha+\beta)a^2/D]^{\pi_3}(\alpha_0 T_m)^{\pi_4}(I_{max}a/k_0 T_m)^{\pi_5}$$
$$(\sigma_0/E)^{\pi_{10}}(\rho D^2/a^2 E)^{\pi_{11}}\}=0 \tag{5.8}$$

Finally, we obtain seven basic dimensionless parameters which are the same as that in expression (2.6) in the following

$$h_1=h/a,\quad A=a\alpha^2/D,\quad B=(\alpha+\beta)a^2/D,\quad h_3=\alpha_0 T_m$$
$$h_4=I_{max}a/k_0 T_m,\quad h_5=E/\sigma_0,\quad h_6=\rho D^2/a^2 E \tag{5.9}$$

In the above expressions, h_1 is the laser-target geometric dimensionless parameter. A and B are the coupled dimensionless parameters which are concerned with the temporal-spatial shape of laser beam and the thermophysical properties of materials. h_3 is the maximum deformable quantity of solid target. h_4 is the coupled dimensionless parameter which is concerned with the laser intensity, geometric parameter and the thermophysical properties of materials. h_5 is the dimensionless parameter of mechanical property of materials. h_6 is the coupled dimensionless parameter which is concerned with the mechanical-thermal properties of materials. From (2.5) and (2.7), we see easily that the temperature rise θ, deflection w, equivalent thermal loading M_t, quasi-static bending moments M_r and M_θ all depend linearly on h_4. This implies that the above physical variables depend linearly on the intensity of the incident laser beam. Meanwhile, w, M_t, M_r and M_θ all depend linearly on h_3. The reason is that M_t, M_r and M_θ result in target deformation, and w reflects the deformable quantity of target. Also, we see that M_t, M_r and M_θ all depend linearly on h_5. In other words, the larger Young's modulus E is and the less yield strength σ_0 is, the more easily the target approches the yield threshold. From (2.5) and (2.7), we also see that each variable depends nonlinearly on h_1, A, B and h_6 respectively. Now supposing that the laser parameters are fixed, we only study the dependence of some physical variables on h_1. The basic parameters of H65 copper alloy for our typical experiment are: $D=0.335\text{cm}^2/\text{s}$, $a=0.25\text{cm}$. Consequently, we have $t_0=0.187\text{s}$, $A=2800$, $B=1.77\times10^4$, $h_6=1.562\times10^{-11}$ and $\nu=0.163$.

2. Thermal moment and quasi-static bending moments

[3] shows that the thermal moment M_t is the key factor to induce the early motion, i. e., the RBM. Fig. 1 displays histories of M_t at the point $r=0$ with different values of h_1. A comparison of Fig. 1 with Fig. 3 and Fig. 4 in [3] shows that the temperature difference of both surfaces and the thermal moment reach simultaneously maximum values. Additionally, when the temperature distribution in axial direction comes into close agreement, the thermal moments diminish to zero. Meanwhile, the less h_1 is, the shorter t_a is, where t_a is the time, when M_t takes effect on the RBM. The more h_1 is the longer t_a is.

Fig. 2 shows the variations of T_{max1} and T_{max2} with h_1^{-1}, where T_{max1} and T_{max2} are, respectively, the time when M_t at the point $r=0$ and $\dfrac{\partial M_t}{\partial r}$ on the rim of laser spot reach their maximum values. It is seen easily that T_{max1} and T_{max2} are inversely proportional to h_1^{-1}. Fig. 3 shows the variation of $M_{t\,max}$ with h_1^{-1}, where $M_{t\,max}$ is the maximum value of M_t at the point $r=0$. From this figure, we see that M_t increases with the increasing of h_1^{-1} when $h_1^{-1}<15$. However, M_t decreases with the increasing of h_1^{-1} when $h_1^{-1}>15$. There is a extreme value point of h_1^{-1} for which the incident laser damages the target most effectually.

Fig. 4 displays the variation of M_t with r, where $t=3.7\times10^{-4}$ and $h_1^{-1}=25$. As expected,

the response of M_r across the irradiated target generally follows the temperature distribution and the laser profile. M_r is uniform within the laser spot and drops sharply near the edge of the laser profile. The special distribution of M_r implies that the spatially cylindrical type pulse laser offers a formidable potential for the exhibition of the RPE.

Fig. 5 displays the variation of M_r and M_θ with r, where $t=1.5\times10^{-4}$ and $h_1^{-1}=25$. M_r is uniform within the laser spot and decrease gradually to zero near the edge of laser spot. However, the characteristic of M_θ is very different from that of M_r. M_θ is positive and uniform within the laser spot. However, near the edge of laser spot, M_θ drops sharply to minimum negative value and then increases gradually to zero. The extraordinary feature of M_r and M_θ demand us to investigate emphatically the characteristics of deformation near the edge of the laser spot.

3. The analysis of deformation

The results of numerical analysis of the RBM are graphically displayed in the figures which follow. The analysis of the RBM include quasi-static deformation w_s, dynamical deflection w_d, total deflection w and their velocity $\frac{\partial w_s}{\partial t}$, $\frac{\partial w_d}{\partial t}$, $\frac{\partial w}{\partial t}$ and gradient $\frac{\partial w}{\partial r}$, $\frac{\partial w_s}{\partial r}$, $\frac{\partial w_d}{\partial r}$.

Fig. 6 (a) and (b) display, respectively, two and three dimensional deflected shape of the middle plane of a thin plate, where $h_1^{-1}=25$. In the geometric configuration of the structure, discribed in Fig. 3 in [3], the deflection value is positive if the thin plate deflects in the same direction as the laser incident direction. The negative values of deflection in the early stage of laser irradiation show that the middle plane of the thin plate bulges in the direction opposite to the laser incident direction. The maximum value of w is 0.26, obtained from Fig. 6 (a). The corresponding factual deflection is $1.84h$ in the case of $h_3=0.0155$ and $h_4=66.4$, where, we observed that the specimen had exhibited the RPE. The prediction of the RBM presented here agrees qualitatively with the experimental observation.

Fig. 7 displays the histories of w_s, w_d and w at the point $r=0$, where $h_1^{-1}=25$. It is seen that the contribution of w_s to the RBM takes positive effect during the whole period of laser irradiation. However, the contribution of w_d to the RBM takes negative effect at the beginning of laser irradiation. Meanwhile, the dynamical deflection induces flexural vibration. Fig. 8 shows the variation of $w_{s\max}$, $w_{d\max}$ and $w_{\max}$ with h_1^{-1}, where $w_{s\max}$, $w_{d\max}$ and $w_{\max}$ are, respectively, the maximum values at point $r=0$. $w_{s\max}$ increase rapidly with the increasing of h_1^{-1}. $w_{d\max}$ increase slowly with the increasing of h_1^{-1}. Therefore, h_1 has important effect on the RBM.

Fig. 9 displays the histories of $\frac{\partial w}{\partial t}$, $\frac{\partial w_s}{\partial t}$ and $\frac{\partial w_d}{\partial t}$ at the point $r=0$. Note that the characteristics of the velocity shown in Fig. 9, and the deflection shown in Fig. 8 are identical. Fig. 9 shows that $\frac{\partial w_{\max}}{\partial t}=16.5$ and $\frac{\partial^2 w_{\max}}{\partial t^2}=2.2\times10^5$. The corresponding factual velocity and acceleration are, respectively, 6.2m/s and 4.53×10^5m/s^2 in the case of $h_3=0.0155$ and $h_4=66.4$, where, we observed that the specimen had exhibited the RPE.

Fig. 10 displays the variations of $\frac{\partial w}{\partial r}$, $\frac{\partial w_s}{\partial r}$ and $\frac{\partial w_d}{\partial r}$ with r. Because of the spatially cylindrical distribution of the laser shape, temperature and equivalent thermal

loading, the deflection gradients have a point of inflection which is on the rim of laser spot. Although the above numerical results and experimental observation show that the deflection is not quite large, the discontinuities of $\frac{\partial^2 w}{\partial r^2}$ on the rim of laser spot demand us to consider the effect of membrane forces.

VI. Concluding Remarks

The RBM on the newly-discoversed RPE is examined by using the uncoupled thin plate theory. Meanwhile, the equivalent thermal loading was presented. The dimensionless analysis of the thin plate motion at the early stage of laser irradiation is given. Numerical results presented show that the rim of laser spot is an extraordinary region which we should emphatically study.

Whereas, the plate material properties have been assumed to be independent of temperature in this study. For the situation with large temperature variation, especially on the rim of laser spot, it will be necessary to account for temperature-dependent properties. This effect, along with the inclusion of thermomechanical coupling in the heat conduction equation and the membrane forces and the shear forces, will be dealt with in forthcoming papers.

Acknowledgement This work was supported by the Field of Laser Technology of the National High-Tech Research and Development Programme, i. e., the 863 Plan.

References

[1] Duan Zhuping and Zhou Yichun, The reverse-plugging effect in metallic foils induced by pulse laser beam, *Advance in Mechanics*, **23**, 1 (1993), 11. (in Chinese)

[2] Duan Zhuping, Zhou Yichun and Wang Chunqui, the reverse-plugging effect in metallic foils induced by non-Gaussian pulsed laser beam, Proceedings of the Symposium on Laser Thermal and Mechanical Effects, Chengdu (1992), 434－453. (in Chinese)

[3] Zhou Yichun, Duan Zhuping and Wang Chunqui, Analytical study on the laser induced reverse-plugging effect by using classical elastic plate theory (I)—Temperature fields, *Applied Mathematics and Mechanics*, **16**, 10 (1995), 913－924.

[4] B. A. Boley and J. H. Weiner, *Theory of Thermal Stresses*, Wiley, New York (1960).

[5] S. Das, Vibrations of polygonal plates due to thermal shock, *J. Sound Vibrat.*, **89** (1983), 471－476.

[6] T. R. Tauchert, Thermal shock of orthotropic rectangular plates, *J. Thermal Stresses*, **12** (1989), 241－258.